Chromatin condensation regulates endothelial cell adaptation to shear stress

Brooke E. Danielsson[a], Katie V. Tieu[a], Stephen T. Spagnol[b], Kira K. Vu[a], Jolene I. Cabe[a], Tristan B. Raisch[a], Kris Noel Dahl[b,c], and Daniel E. Conway[a,d,e,*]

[a]Department of Biomedical Engineering, Virginia Commonwealth University, Richmond, Virginia 23284; [b]Department of Chemical Engineering, Carnegie Mellon University, Pittsburgh, PA 15213; [c]Forensics Department, Thornton Tomasetti, New York City, NY 10271; [d]Department of Biomedical Engineering, [e]Center for Cancer Engineering, and Arthur G. James Comprehensive Cancer Center, The Ohio State University, Columbus, OH 43210

ABSTRACT **Vascular endothelial cells (ECs) have been shown to be mechanoresponsive to the forces of blood flow, including fluid shear stress (FSS), the frictional force of blood on the vessel wall. Recent reports have shown that FSS induces epigenetic changes in chromatin. Epigenetic changes, such as methylation and acetylation of histones, not only affect gene expression but also affect chromatin condensation, which can alter nuclear stiffness. Thus, we hypothesized that changes in chromatin condensation may be an important component for how ECs adapt to FSS. Using both in vitro and in vivo models of EC adaptation to FSS, we observed an increase in histone acetylation and a decrease in histone methylation in ECs adapted to flow as compared with static. Using small molecule drugs, as well as vascular endothelial growth factor, to change chromatin condensation, we show that decreasing chromatin condensation enables cells to more quickly align to FSS, whereas increasing chromatin condensation inhibited alignment. Additionally, we show data that changes in chromatin condensation can also prevent or increase DNA damage, as measured by phosphorylation of γH2AX. Taken together, these results indicate that chromatin condensation, and potentially by extension nuclear stiffness, is an important aspect of EC adaptation to FSS.**

Monitoring Editor
Dennis Discher
University of Pennsylvania

Received: Feb 28, 2022
Revised: Jul 11, 2022
Accepted: Jul 20, 2022

INTRODUCTION

Structures within the nucleus, including chromatin, lamins, and other genomic elements, are highly adaptable and can assume various structural morphologies. Epigenetic changes to the chromatin, such as acetylation and methylation of histones, alter compaction and configuration (Goldberg *et al.*, 2007). Decondensed chromatin has been shown to have heightened mobility, reduced stiffness, and is frequently associated with gene-rich regions of euchromatin (Chubb *et al.*, 2002; Mearini and Fackelmayer, 2006). In contrast, condensed chromatin exists as a more compacted structure, frequently associated with gene-poor regions of heterochromatin (Küpper *et al.*, 2007; Fedorova and Zink, 2009; Dahl *et al.*, 2010; Geyer *et al.*, 2011). Changes in chromatin compaction can modulate overall nuclear shape, volume, and stiffness (Furusawa *et al.*, 2015; Damodaran *et al.*, 2018; Stephens *et al.*, 2018). Mechanical measurements of the nucleus have shown that the viscoelastic nature of chromatin acts as the dominant mechanical element of the nuclear interior when a nucleus deforms under high strain (Pajerowski *et al.*, 2007; Spagnol *et al.*, 2016).

Vascular endothelial cells (ECs) are continually exposed to mechanical forces as a result of blood flow, which include both fluid shear stress and cyclic stretch. Both in vivo and in vitro studies of EC responses to fluid shear stress have shown that atheroprotective shear stress (unidirectional laminar shear stress [LSS]) induces a cellular response in EC whereby cells adapt to the forces of fluid flow by aligning both the EC nucleus and actin filaments in the direction of flow. However, EC exposed to atheroprone shear stress

This article was published online ahead of print in MBoC in Press (http://www.molbiolcell.org/cgi/doi/10.1091/mbc.E22-02-0064) on July 27, 2022.

*Address correspondence to: Daniel E. Conway (conway.362@osu.edu).

Abbreviations used: EC, endothelial cells; FSS, fluid shear stress; H3K9ac, acetylation at the ninth lysine residue of histone 3; H3K9me$_3$, trimethylation at the ninth lysine residue of histone 3; H3K27me$_3$, trimethylation at the 27th lysine residue of histone 3; LSS, laminar shear stress; OSS, oscillatory shear stress; TSA, trichostatin A; VEGF, vascular endothelial growth factor.

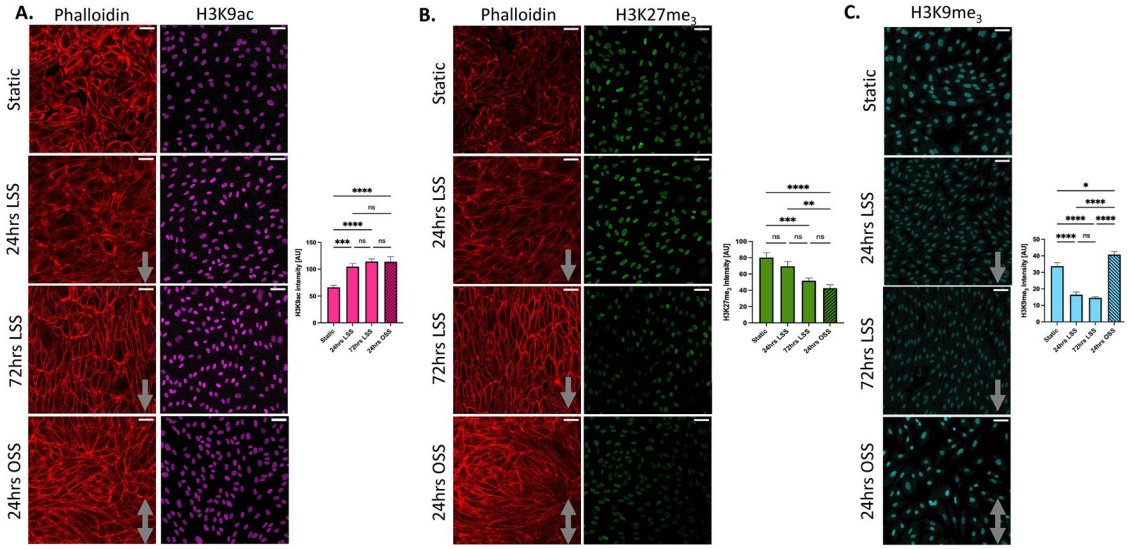

FIGURE 1: Epigenetic modifications in response to fluid shear stress in vitro. Representative phalloidin and histone epigenetic markers (H3K9ac, H3k27me3, H3k9me3) images and quantification of untreated ECs exposed to 12 dynes/cm^2 laminar and oscillatory shear stress. Confocal images taken on a 20× confocal microscope. Gray arrows indicate flow direction. Scale bar = 50 μm. (A) Laminar shear stress causes an increase in H3K9ac expression in aligned ECs adapted to flow. The graph quantifies the mean fluorescent intensity of histone marker H3K9ac ($n = 3$; ****, $p < 0.0001$; ***, $p = 0.0004$; ns, nonsignificant; ordinary one-way ANOVA with SEM/ Tukey's multiple comparisons). (B) Laminar shear stress causes a decrease in H3K27me3 expression in aligned ECs adapted to flow. The graph quantifies the mean fluorescent intensity of histone marker H3K27me3 ($n = 3$; ****, $p < 0.0001$; ***, $p = 0.0008$; **, $p = 0.0016$; ns, nonsignificant; ordinary one-way ANOVA with SEM/ Tukey's multiple comparisons). (C) Laminar shear stress causes a decrease in H3K9me3 expression in aligned EC adapted to flow. The graph quantifies the mean fluorescent intensity of histone marker H3K9me3 ($n = 3$; ****, $p < 0.0001$; *, $p = 0.0188$; ns, nonsignficant; ordinary one-way ANOVA with SEM/ Tukey's multiple comparisons).

(multidirectional, oscillating shear stress [OSS]), this alignment response does not occur, with random orientation of cellular alignment. The alignment EC to shear stress is considered to be an important aspect of cellular adaptation to fluid shear stress, and is frequently correlated to differences in gene expression and inflammatory markers (Hahn and Schwartz, 2009).

Previous publications have studied epigenetic changes for ECs exposed to fluid shear stress (Illi *et al.*, 2003; Chen *et al.*, 2008; Lee *et al.*, 2012, 2017; Dunn *et al.*, 2014; Zhou *et al.*, 2014; Jiang *et al.*, 2015; Ku *et al.*, 2019; Lee and Chiu, 2019). It has been shown that OSS induces expression of DNA methyltransferases (DNMTI; Zhou *et al.*, 2014; Dunn *et al.*, 2015a), as well as up-regulates histone deacetylases (Chen *et al.*, 2008; Lee *et al.*, 2012) in comparison to LSS both in vivo and in vitro. A major focus of these studies has been how epigenetic changes affect gene expression. However, it remains possible that these epigenetic changes can also affect the mechanical state of the nucleus. Prior studies have shown that direct force generated on cells influences chromatin organization (Hampoelz *et al.*, 2011; Booth-Gauthier *et al.*, 2012; Iyer *et al.*, 2012; Spagnol and Dahl, 2014). Additionally, these nuclear mechanical changes may not only affect how cells sense and respond to mechanical forces but may also be a critical aspect in the prevention of DNA damage (Zink *et al.*, 2004; Isermann and Lammerding, 2013; Denais *et al.*, 2016). For example, Nava *et al.* showed, in an epithelial stretch model, that adaptations in chromatin architecture and rheology are required to prevent DNA damage in cells exposed to mechanical force (Nava *et al.*, 2020).

We hypothesized that chromatin condensation could represent an important aspect for how EC adapt to and align in the direction of shear stress. By examining changes in epigenetic histone markers, we identified H3K9ac, H3K27me$_3$, and H3K9me$_3$ as sensitive to fluid shear stress, indicating that there are substantial changes in chromatin acetylation and methylation in cells adapted to either atheroprotective or atheroprone shear stress. We also show that increasing histone acetylation increases the speed by which ECs align to fluid shear stress, whereas increasing histone methylation inhibited EC alignment to fluid shear stress. Lastly, by measuring γH2AX foci, we show that DNA damage in response to fluid shear stress is sensitive to changes in chromatin condensation. Taken together, our data identify chromatin condensation as an important biophysical parameter for EC adaptation to fluid shear stress.

RESULTS

Endothelial cells adapted to shear stress have altered histone acetylation and methylation indicative of increased chromatin decondensation

We sought to understand how chromatin condensation changes in ECs adapted to LSS. HUVECs were exposed to laminar and oscillatory shear stress at physiological levels of arterial shear stress (12 dynes/cm^2; Cunningham and Gotlieb, 2005) and assayed for histone markers H3K9ac, H3K27me$_3$, and H3K9me$_3$. H3K9ac is an epigenetic marker for histone acetylation, indicating chromatin decondensation (Berger *et al.*, 2020). H3K27me$_3$ and H3K9me$_3$ are epigenetic markers for histone methylation, indicating chromatin condensation (Igolkina *et al.*, 2019).

We observed that as EC remodeling occurs (indicated by actin alignment in the direction of flow), H3K9ac expression increases (Figure 1A) and H3K27me$_3$ expression decreases (Figure 1B), showing that ECs adapted to LSS have increased chromatin decondensation. H3K9ac expression was not changed at earlier timepoints of shear stress (30 min to 8 h), whereas H3K27me$_3$ had a transient increase from 30 min to 4 h (Supplemental Figure 1).

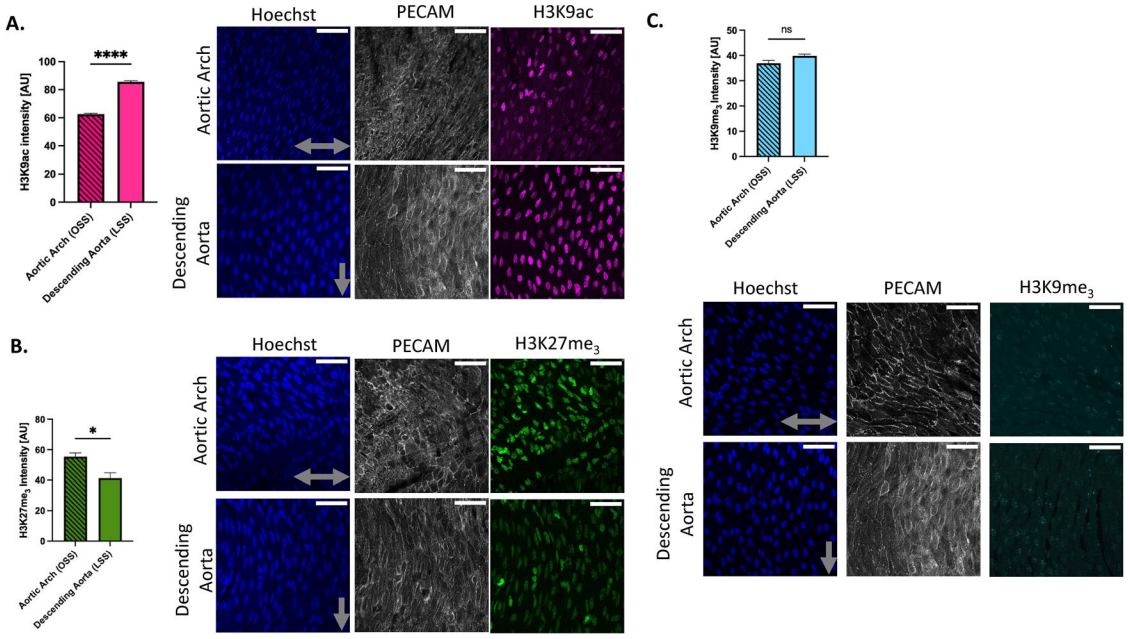

FIGURE 2: Epigenetic modifications in response to fluid shear stress in vivo. Representative Hoechst, PECAM, and histone epigenetic markers (H3K9ac, H3K27me$_3$) images and quantification of harvested mouse aortic tissue. Confocal images taken on a 40× confocal microscope with water immersion. Gray arrows indicate flow direction. Scale bar = 50 μm. (A) H3K9ac expression was higher in vascular region of laminar shear stress (descending aorta) than in regions of oscillatory flow (aortic arch). The graph quantifies the mean fluorescent intensity of histone marker H3K9ac (samples harvested from three mice; ****, $p < 0.0001$; paired, two-tailed *t* test with SEM). (B) H3K27me$_3$ expression was higher in vascular regions of oscillatory flow (aortic arch) than in regions of laminar shear stress (descending aorta). The graph quantifies the mean fluorescent intensity of histone marker H3K27me$_3$ (samples harvested from three mice; *, $p < 0.05$; paired, two-tailed *t* test with SEM). (C) No significant difference was observed in H3K9me$_3$ expression between the descending aorta and the aortic arch. The graph quantifies the mean fluorescent intensity of histone marker H3K9me$_3$ (samples harvested from three mice; ns, nonsignificant; paired, two-tailed paired *t* test with SEM).

To determine whether alignment, including actin remodeling, is necessary for changes in H3K9ac and H3K27me$_3$, we performed shear stress experiments in the presence of 5 μM Y-27632, previously shown to inhibit shear stress–induced actin realignment (Wojciak-Stothard and Ridley, 2003; van der Meer *et al.*, 2010). Cells treated with Y-27632 did not exhibit shear stress–induced changes in H3K9ac or H3K27me$_3$. These data suggest that increased H3K9ac expression and decreased H3K27me$_3$ expression is part of a longer-term adaptation to shear stress rather than a short-term response.

Under oscillatory flow, H3K9ac expression was higher than H3K27me$_3$ expression (Figure 1, A and B). This result was surprising due to prior reports of increased methylation in regions of oscillatory flow (Zhou *et al.*, 2014; Dunn *et al.*, 2015b) in vitro as well as in vivo. We also examined H3K9me$_3$ expression, as expression of this marker was found to be corelated to nuclear stiffness in epithelial cells (Nava *et al.*, 2020). In our in vitro endothelial shear model, we found that ECs exposed to LSS had decreased H3K9me$_3$ expression compared with ECs in static culture (Figure 1C). Under oscillatory flow, however, H3K9me$_3$ expression increased (Figure 1C).

Endothelial cells adapt to shear stress in vivo through chromatin decondensation

Next, we sought to examine chromatin condensation in vivo by comparing histone acetylation and methylation changes of mouse ECs in the descending aorta to the inner curvature of the aortic arch. ECs in the descending aorta experience LSS, whereas EC in the inner curvature of the aortic arch experience OSS (Suo *et al.*, 2007). Our in vivo findings mirrored our in vitro findings in that ECs adapted to LSS have an increase in H3K9ac expression. We observed that ECs located in the descending aorta had more H3K9ac expression than the ECs located in the aortic arch (Figure 2A). This suggests that chromatin decondensation is associated with ECs adapted shear stress in vivo as well as in vitro. In contrast, H3K27me$_3$ expression was higher in the aortic arch than in the descending aorta (Figure 2B). This result was different than the EC histone modification expression in the in vitro model where H3K27me$_3$ was lower under OSS flow. When we looked at H3K9me$_3$ expression we saw no significant difference between the two regions of flow (Figure 2C).

Chromatin decondensation leads to faster EC actin alignment under LSS

ECs were treated with histone deacetylase inhibitor, TSA, which has been previously shown to increase euchromatin (Yoshida *et al.*, 1990; Fejes Tóth *et al.*, 2004), whereas histone demethyltransferase inhibitor, methylstat, has been shown to increase heterochromatin (Luo *et al.*, 2011). To confirm TSA and methylstat were causing the desired histone modifications in our EC model, we did immunofluorescent staining and quantified fluorescent intensity of H3K9ac for histone 3 acetylation, and H3K27me$_3$ for histone 3 methylation. H3K9ac expression was increased in ECs treated with 100 nM TSA for 24 h (Figure 3B), confirming that TSA causes chromatin decondensation. H3K27me$_3$ expression was increased in ECs treated with 2.5 μM methylstat for 48 h (Figure 3B), confirming methylstat causes chromatin condensation.

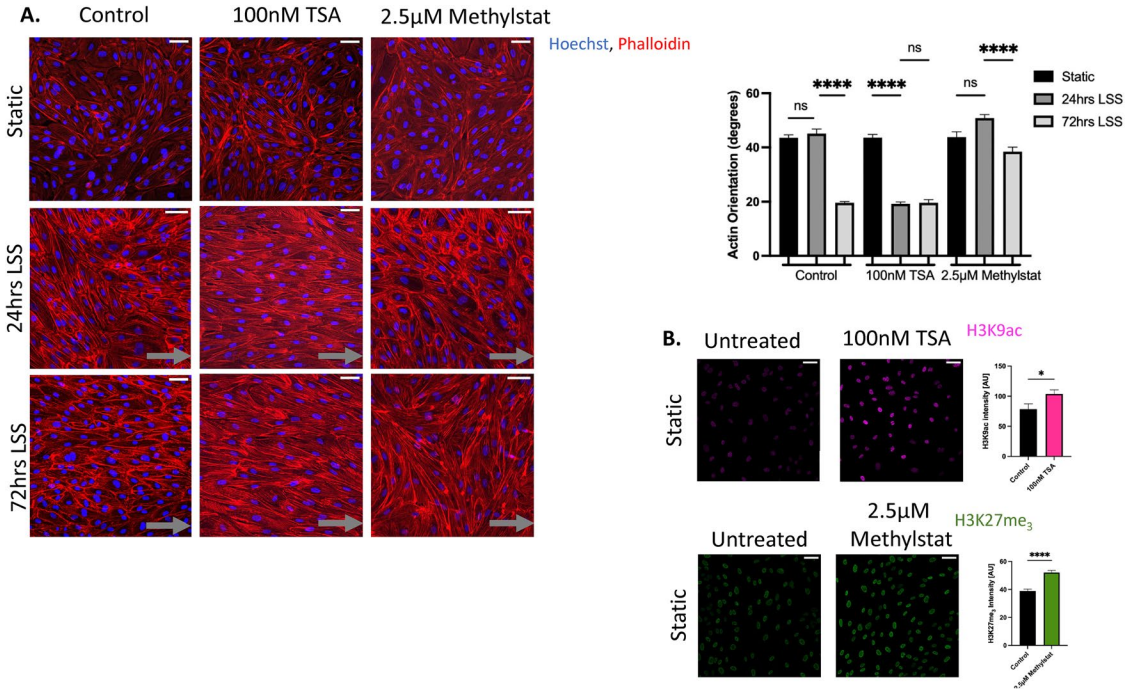

FIGURE 3: Chromatin decondensation increases the rate of EC alignment to shear stress. (A) Representative phalloidin and Hoechst images and quantification of EC exposed to 12 dynes/cm^2 laminar shear stress. Confocal images taken on a 20× confocal microscope. Gray arrows indicated flow direction. Scale bar = 50 μm. Chromatin decondensation through TSA treatment facilitates actin alignment 48 h faster than untreated ECs under shear stress. Chromatin condensation through methylstat treatment blocks EC adaptation by inhibiting actin remodeling under shear stress. Actin orientation was quantified by fiber degrees. Static orientation is at 45° (data represents average per frame with 10 frames per experiment; ****, $p < 0.0001$, ns, nonsignificant; ordinary one-way ANOVA with SEM/ Tukey's multiple comparisons). (B) Representative histone epigenetic markers (H3K9ac, H3K27me$_3$) images and quantification showing chromatin condensation changes due to EC treatment with TSA (increase in H3K9ac) and methylstat (increase in H3K27me$_3$) compared with untreated controls. Confocal images taken on a 20× confocal microscope. Scale bar = 50 μm. The graph quantifies the mean fluorescent intensity of histone markers H3K9ac and H3K27me ($n = 3$; ****, $p < 0.0001$, $p = 0.4428$; two-tailed paired *t* test with SEM).

To see how induced chromatin decondensation or condensation effects EC adaptation to flow, we examined how treatment with TSA or methylstat affected EC alignment. ECs were exposed to static culture, as well as 12 dynes/cm^2 of laminar shear stress for 24 or 72 h. Actin alignment was quantified by the mean actin orientation in degrees, where closer to 0° is more aligned in the direction of flow, and 45° is random orientation (as seen in static conditions). Untreated ECs showed complete actin alignment in the parallel direction of flow by 72 h of shear stress; however, TSA-treated cells were completely aligned after only 24 h of shear stress (Figure 3A). In contrast, cells treated with methylstat did not align even after exposure to 72 h of shear stress (Figure 3A). Taken together, these results show that changes in chromatin organization affect EC adaptation to flow.

VEGF decondenses chromatin and causes faster EC alignment

Next, to examine a more physiological treatment, we examined the effects of VEGF, a signal protein that stimulates angiogenesis, on both chromatin condensation and EC alignment. Prior work, using particle-tracking microrheology, showed that VEGF treatment resulted in a more decondensed chromatin structure (Spagnol and Dahl, 2014). Using fluorescence lifetime measurements to characterize chromatin condensation state (Spagnol and Dahl, 2016), we examined the effects of VEGF treatment on EC chromatin mobility. We observed an increasing number of high mean fluorescence lifetime regions within the nucleus with increasing duration (1–2.5 h) of VEGF exposure consistent with a growing number of regions of decondensed chromatin (Figure 4A). At later times, we qualitatively observe a combination of low and very high mean fluorescence lifetime regions consistent with regions of both condensed chromatin and decondensed chromatin, respectively. Next, we examined whether VEGF treatment would also accelerate EC alignment to LSS. We observed VEGF treated ECs aligned faster to LSS (Figure 4B), mirroring the results of TSA treatment (Figure 3A).

Chromatin drug treatments do not disrupt cell–cell adhesions, focal adhesions, nuclear structure, or inhibit gene transcription

Because the drug treatments used in Figures 3 and 4 likely have additional effects on ECs beyond regulation of chromatin condensation, we examined whether these drug treatments disrupted cell–cell adhesions or focal adhesions, two critical structures of the cell responsible for adaptation to fluid shear stress (Hahn and Schwartz, 2009). Treatment with TSA, methylstat, or VEGF did not appear to dramatically affect cell–cell adhesions (assessed with VE-cadherin immunostaining) or focal adhesions (assessed with β1 integrin staining; Supplemental Figure 3), suggesting that these mechanosensitive structures are not disrupted by the drug treatments. Additionally, we did not observe any changes in lamin A/C immunostaining

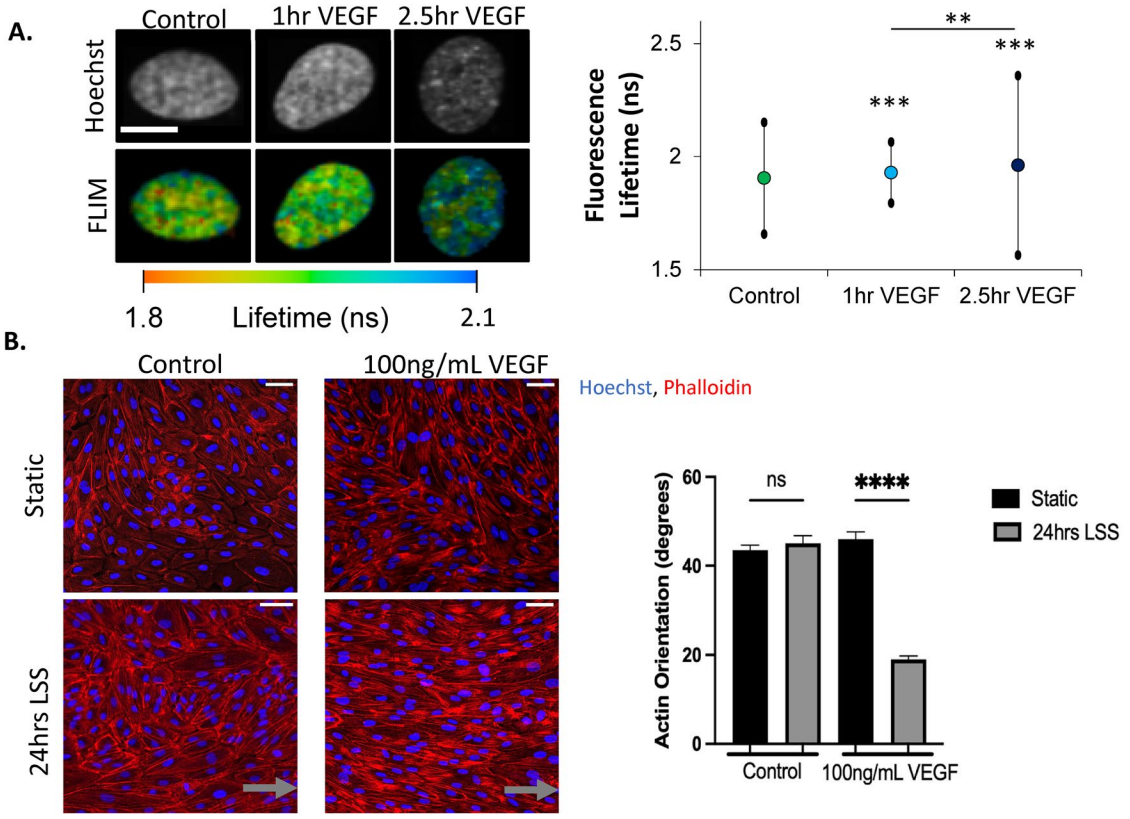

FIGURE 4: VEGF treatment increases chromatin decondensation and increases the rate of EC alignment to shear stress. (A) Fluorescence lifetime measurements of chromatin condensation state during stimulated gene activation in VEGF-stimulated endothelial cell nuclei. Fluorescence intensity confocal images (top) and mean fluorescence lifetime heat maps (bottom) of chromatin in EC nuclei labeled with Hoechst 33342 and treated with 50 ng/ml VEGF for 0, 1. or 2.5 h. Mean fluorescence lifetime heat maps indicate spatial arrangement of local fluorophore environments for stained chromatin, which is consistent with varying chromatin condensation state. Altered fluorescence intensity with treatments show differential chromatin condensation state, with more intense fluorescence arising from highly concentrated condensed chromatin. The graph shows treatment with VEGF at both timepoints resulted in a strong and statistically significant increase in the mean fluorescence lifetime relative to untreated controls (***, $p \ll 0.001$), with a stepwise increase at each timepoint (**, $p < 0.025$). Analysis was done using 60–80 segmented nuclei for each treatment condition. Error bars indicate SD of pixel-to-pixel mean fluorescence lifetime differences of segmented nuclei under each treatment condition. Scale bar is 10 μm. (B) Chromatin decondensation through VEGF treatment facilitates actin alignment 48 h faster than untreated ECs under shear stress. Representative phalloidin and Hoechst images and quantification of untreated ECs exposed to 12 dynes/cm^2 laminar shear stress. Confocal images taken on a 20× confocal microscope. Gray arrows indicate flow direction. Scale bar = 50 μm. Actin orientation was quantified by fiber degrees. Static orientation is at 45° (data represents average per frame with 10 frames per experiment; ****, $p < 0.0001$; ns, nonsignificant; ordinary one-way ANOVA with SEM/ Tukey's multiple comparisons).

(expression or nuclear morphology) with these drug treatments (Supplemental Figure 4). Lastly, we investigated whether any of the drug treatments might be inhibiting global transcription changes induced by shear stress. We used H3K4me$_3$ as a marker of transcriptionally active genes. In static culture we observed no changes in H3K4me$_3$ with drug treatments (Supplemental Figure 5). Interestingly, we observed that all three drug treatments increased H3K4me$_3$ expression in cells exposed to shear stress when compared with untreated cells. Although this may indicate that the drugs may result in increased transcriptional activity in cells exposed to shear stress, it does suggest that the drug treatments do not inhibit transcription changes required for adaptation to shear stress. In summary, while these drugs may affect other processes beyond chromatin condensation, these control experiments further support the hypothesis that these drugs mediate EC alignment as a result of changes in chromatin condensation.

Changes in chromatin condensation affect shear stress–induced DNA damage

We next examined how changes in chromatin condensation would affect shear stress–nduced DNA damage. Untreated control cells, when fully aligned to fluid shear stress (72 h), had less γH2AX foci detected by immunofluorescence as compared with static culture (Figure 5A), consistent with a prior report showing that fluid shear stress increases expression of p53, potentially enhancing DNA repair (Lin *et al.*, 2000). When cells were treated with TSA to decondense chromatin, a further reduction in γH2AX foci was observed in both static and LSS conditions. Interestingly, methylstat treatment increased DNA damage most significantly in cells exposed to LSS. In similar experiments, cells were exposed to OSS after treatment with TSA or methylstat. OSS induced the most DNA damage in TSA-treated ECs (Figure 5B). Thus, changes in chromatin condensation not only affect EC alignment but also affect DNA damage.

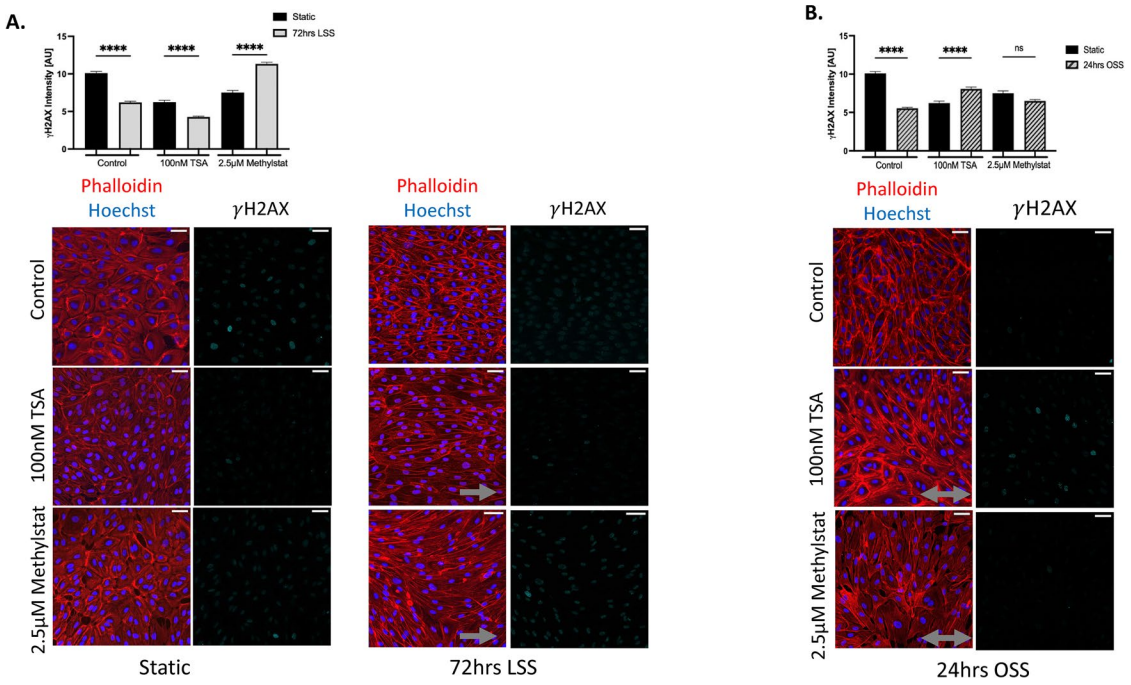

FIGURE 5: Changes in chromatin condensation affect shear stress–induced DNA damage. Representative phalloidin, Hoechst, and DNA double-stranded DNA damage marker γH2AX. Images and quantification of untreated EC exposed to 12 dynes/cm^2 laminar and oscillatory shear stress. Confocal images taken on a 20× confocal microscope. Gray arrows indicate flow direction. Scale bar = 50 μm. (A) Laminar shear stress in ECs with condensed chromatin (methylstat-treated cells) causes an increase in DNA damage. The graph quantifies the fluorescent intensity of γH2AX foci per nuclei (three experiments with $n > 300$ cells; ****, $p < 0.0001$; ordinary one-way ANOVA with SEM/ Tukey's multiple comparisons). (B) Oscillatory shear stress in ECs with decondensed chromatin (TSA-treated cells) causes an increase in DNA damage. The graph quantifies the fluorescent intensity of γH2AX foci per nuceli (three experiments with $n > 300$ cells; ****, $p < 0.0001$; ns, nonsignificant; ordinary one-way ANOVA with SEM/Tukey's multiple comparisons).

DISCUSSION

In this article we show both in vitro (Figure 1) and in vivo (Figure 2) that fluid shear stress affects histone 3 methylation and acetylation, by examining immunostaining of H3K9ac, H3K27me$_3$, and H3K9me$_3$. Overall, our data suggest that EC exposed to laminar shear stress (atheroprotective) have histones which are more acetylated and less methylated, suggesting a more decondensed chromatin structure in ECs following adaptation to LSS. These changes occur only after longer-term exposure (≥24 h) to shear stress (Supplemental Figure 1), and appear to be dependent on actin reorganization (Supplemental Figure 2), indicating that flow-induced epigenetic changes are downstream from previously characterized shear stress signaling events at cell–cell and cell–ECM adhesions (Tzima *et al.*, 2005). While this data is mostly correlative, we also demonstrate that changes in chromatin condensation with small molecules (Figure 3) and VEGF (Figure 4) significantly affect EC adaptation to shear stress, using EC alignment as a marker for adaptation. Thus, changes in chromatin condensation greatly impact the propensity of cells to align to shear stress. Lastly, we show that changes in chromatin condensation affect markers of DNA damage (Figure 5).

Prior work has also studied the role of histone acetylation and methylation changes during adaptation to shear stress. Early studies showed that short-term exposure (<120 min) LSS induces chromatin remodeling through H3/H4 acetylation (Illi *et al.*, 2003; Chen *et al.*, 2008). Our findings of increased H3K9ac are in agreement with these prior studies, and demonstrate that increased acetylation persists in cells exposed to LSS as compared with static culture (Figures 1A and 2A). More recent work has shown that oscillatory or atheroprone fluid shear stress increases genome-wide DNA methylation patterns in a DNA methyltransferase-dependent (DNMT-dependent) manner (Dunn *et al.*, 2014; Zhou *et al.*, 2014). In this study we observed increases in H3K9me$_3$ (in vitro; Figure 1C) and H3K27me$_3$ (in vivo; Figure 2B) for ECs exposed to OSS as compared with LSS, in agreement with these prior studies showing increased methylation with OSS. However, we observed divergence in the H3 methylation markers up-regulated by shear stress in in vitro versus in vivo experiments. The in vitro versus in vivo differences in H3 methylation markers could be due to differences in the time of exposure to OSS (24 h in vitro vs. months in vivo), with the in vitro results representing an initial response and the in vivo results representing a more terminal response. We also acknowledge that there may be additional factors beyond shear stress that may be regulating histone methylation in the different regions of the aorta.

Although the nuclear lamina is considered to be a major contributor to nuclear stiffness (Butin-Israeli *et al.*, 2012; Dreger *et al.*, 2019), changes in chromatin condensation, as a result of altered histone acetylation and methylation, have been shown to affect nuclear stiffness independent of the nuclear lamins (Stephens *et al.*, 2017, 2018). The changes observed in histone acetylation and histone methylation (Figures 1 and 2) are suggestive of nuclei being softer in ECs exposed to LSS when compared with EC exposed to OSS. We also note that in vitro OSS increased expression of H3K9me$_3$, which has also been previously shown to be a histone marker that correlates to nuclear stiffness (Nava *et al.*, 2020). Thus, it is tempting to speculate that the observed changes in chromatin methylation and acetylation markers are indicative of changes in nuclear stiffness.

We note prior work by Deguchi and colleagues that showed increased nuclear stiffness in ECs aligned to LSS as compared with ECs in static culture (Deguchi *et al.*, 2005). It is not yet known whether there are differences in nuclear stiffness for ECs exposed to LSS versus OSS. Additionally, it is not yet understood how nuclear stiffness may change during earlier timepoints when ECs are actively adapting to shear stress. Nuclear circularity, elongation, and area have already been shown to rapidly change upon exposure to shear stress (Jiang and Ji, 2018), thus it may be possible that nuclear stiffness changes rapidly as well at the onset of flow. Further supporting the requirement for an "adaptable" EC nucleus, our group has shown that ECs with stiffer nuclear lamins cannot adapt to shear stress (Danielsson *et al.*, 2022).

We observed that increasing histone acetylation allowed ECs to align more rapidly to shear stress, whereas increasing histone methylation inhibited EC alignment (Figure 3), demonstrating that chromatin condensation can affect the rate at which ECs adapt to flow. Additionally, similar enhancements of EC alignment can be obtained with a physiological stimulus (VEGF), which also increases chromatin mobility (Figure 4). It is important to consider that VEGF is a potent growth factor, known to affect many EC signaling pathways, and thus it is difficult to ascertain whether the accelerated alignment is exclusively due to increased chromatin decondensation.

One mechanism to explain this enhanced adaptability is that reduced nuclear stiffness, as a result of chromatin condensation, allows for a more rapid change in nuclear shape during the EC alignment process. Prior work using atomic force microscopy has shown that chromatin compaction via TSA treatment resulted in decreased nuclear stiffness by ~35–50% (Krause *et al.*, 2013; Stephens *et al.*, 2017) and that methylstat treatment increased nuclear stiffness by ~40% (Stephens *et al.*, 2018), indicating that these treatments are likely inducing substantial changes to nuclear stiffness to EC in our experiments. We also note that it is well established that significant gene expression changes occur during the process of EC adaptation to shear stress (Hahn and Schwartz, 2009). Thus, an alternative or parallel mechanism to explain the enhanced alignment speed by chromatin decondensation is that decondensed chromatin enhances individual gene expression changes needed for adaptation to shear stress.

An interesting observation of our findings is that changes in chromatin can also influence shear stress–induced DNA damage. Mechanical forces have been shown to induce DNA damage in a wide variety of contexts (Miroshnikova and Wickström, 2022). The Wickström group recently showed that changes in nuclear mechanical properties can counteract the effects of force-induced DNA damage. Specifically, epithelial cells respond to mechanical stretch by decondensing chromatin by reducing chromatin methylation. These changes in chromatin condensation are critical for preventing stretch-induced DNA damage (Nava *et al.*, 2020). Our work shows similar findings in the context of LSS. ECs with decondensed chromatin have less DNA damage when exposed to LSS (Figure 5A). Interestingly, our findings were opposite with OSS, where ECs with a more condensed chromatin experienced less DNA damage (Figure 5B). In some cases, increased chromatin rigidity has been shown to provide genome protection (Stephens, 2020). It therefore appears that the relationship between EC chromatin condensation and DNA damage varies depending on the type of mechanical force (LSS vs. OSS).

In conclusion, this study demonstrates that chromatin condensation is not only regulated by fluid shear stress, but is a critical parameter that regulates EC mechanoadaptation to fluid shear stress. There are likely many physiologically and pathologically relevant processes, such as inflammation, that regulate EC chromatin condensation, and in turn have the potential to alter EC adaptation to shear stress, as well as force-induced DNA damage. It will be interesting to determine the role of chromatin condensation in other potential mechanosensitive EC processes, such as angiogenesis.

MATERIALS AND METHODS

Request a protocol through *Bio-protocol*.

Cell type

Commercially available primary human umbilical vein endothelial cells (HUVECs; pooled, passages 3–5; Lonza, Basel, Switzerland) grown in EGM-2 medium (Lonza, Basel, Switzerland) was used for all experiments.

Chromatin condensation modifications

For epigenetic modifications, HUVECs were treated with histone deacetylase inhibitor, 100 nM trichostatin A (TSA; Cayman Chemical Company), to increase euchromatin, and a histone demethyltransferase inhibitor, 2.5 μM methylstat (Sigma-Aldrich), to increase heterochromatin. In addition, we also used 50–100 ng/mL vascular endothelial growth factor (VEGF; Peprotech) for 24 h for shear experiments, and 1–2.5 h for FLIM experiments.

Fluid shear stress

HUVECs were seeded onto ibidi chamber slides (ibidi-treated μ-slides $I^{0.4\ or\ 0.6}$, cat. #80186 or ibidi-treated μ-slides $VI^{0.4}$, cat. #80606, Germany), coated with 60 μg/ml fibronectin (Sigma-Aldrich; F1141). At 80% confluency, HUVECs were exposed to laminar (steady 12 dynes/cm^2) or oscillatory (0 ± 12 dynes/cm^2, 1 Hz) shear stress using the ibidi pump system (ibidi; cat. #10902; Germany) with or without drug treatments (as indicated in figure legends) perfused in the media.

Cell fixation and immunofluorescence staining

HUVECs were washed two times with phosphate-buffered saline (PBS) and fixed for 10 min at room temperature with 4% paraformaldehyde in PBS. After three washes with PBS, the cells were permeabilized for 10 min at room temperature with 0.2% Triton X-100 in PBS and blocked with 5% bovine serum albumin for 1 h at room temperature. Cells were then incubated overnight at 4°C room temperature with the primary Ab diluted in blocking solution. The following primary antibodies were used: H3K9ac (Cell Signaling 9649; 1:400), $H3K27me_3$ (Cell Signaling 9733; 1:1000), $H3K9me_3$ (Cell Signaling 13969; 1:100), $H3K4me_3$ (Cell Signaling 9751; 1:400), phospho-histone H2A.X (Ser139; Cell Signaling 9718; 1:400), CD29 Integrin beta 1 (Thermo Scientific; 14-0299-82; 1:100), lamin A/C (Santa Cruz Biotechnology; sc-7292; 1:100), or VE-cadherin (Cell Signaling Technology; D87F2; 1:250). Three more washes with PBS were then followed by incubation with the secondary Ab (Alexa Fluor 647–conjugated donkey anti-rabbit IgG; Thermo Fisher) and stained with rhodamine phalloidin (cat. # PHDR1; Cytoskeleton) for 45 min followed by three additional PBS washes. Samples were stained with Hoechst 33342 (Thermo Fisher) and mounted with ibidi mounting medium (ibidi; cat. #50001; Germany).

Mouse aorta preparation and immunohistochemistry

All animal studies were approved by the Virginia Commonwealth University Institutional Animal Care and Use Committee (protocol #AD10002187) and performed in accordance with the Guide for the Care and Use of Laboratory Animals. Mice were euthanized by CO_2 inhalation followed by cervical dislocation. The mouse heart was immediately perfused with saline solution containing heparin (Tocris Bioscience; 28-12100) and then were perfusion-fixed with

either 10% formalin (Sigma-Aldrich; HT501320) or 100% methanol (Fisher Scientific; BP28184). The aortas, arch, and descending thoracic, were then harvested, cleaned in situ and then transferred to a 12-well dish containing saline. *En face* preparation and immunohistochemistry of the tissue was preformed using previously described methods (Ko *et al.*, 2017).

The aortic arch and thoracic aorta were separated and dissected, then permeabilized with 0.1% Triton X-100 (Sigma-Aldrich; X100-500 ml) for 10 min at room temperature or 100% ice-cold methanol at –20°C for 10 min. All washing steps were done by washing three times with TBST-1X rocking at room temperature for 10 min each time. The samples were blocked with 10% normal donkey serum (Abcam; 7475) in 1X Tris buffered saline with Tween 20 (TBST) diluted from TBST-10X (Cell Signaling; 9997) using ddH_2O for 30 min with rocking at room temperature. Primary antibodies were diluted in TBST-1X with 10% normal donkey serum overnight in 4°C. The following primary antibodies were used: H3K9ac (Cell Signaling; 9649; 1:400), $H3K27me_3$ (Cell Signaling; 9733; 1:1000), $H3K9me_3$ (Cell Signaling; 13969;1:100), and PECAM-1 (Santa Cruz Biotechnology; sc-18916; 1:250). After washing, the tissues were fluorescently labeled with secondary antibodies diluted in TBST-1X with 10% normal donkey serum for 1 h, rocking in room temperature. The following secondary antibodies were used: chicken anti-rat 647 (Invitrogen; A21472), donkey anti-rabbit 568 (Invitrogen; A10042), and donkey anti-rabbit 647 (Thermo Scientific; A31573). Next, nuclear staining was done with Hoechst (Invitrogen; H3570) diluted in TBST-1X (1 µl: 10 ml) and incubated with rocking at room temperature for 30 min. After washing, the tissues were mounted onto glass slides and sealed with ProLong Gold Antifade (Invitrogen; P36930).

Microscopy and image analysis

Fixed samples were imaged on a Zeiss LSM 710 or LSM 980 (Airyscan) confocal microscope at 20×, 40×, or 63× with water or oil immersion. Histone modifications were quantified based on fluorescence intensities as previously described (Nava *et al.*, 2020) using Fiji ImageJ. The orientation of actin fibers was measured using a custom MATLAB program. The phalloidin channel of each image was selected, then sharpened and despeckled using the "imsharpen," "edge," and "bwareaopen" MATLAB commands to isolate the actin fibers. The "regionprops" command was then used to measure the orientation of each region—the isolated actin fibers. The orientation of these fibers was then averaged, and the averaged orientations are reported. A randomly distributed arrangement of fibers should have an average orientation of about 45°, which is what was observed in our static samples. An average orientation closer to zero is representative of fibers which are more oriented in the direction of fluid flow.

Fluorescence lifetime imaging microscopy

Our FLIM setup utilized a Leica TCS SP5 inverted laser scanning confocal microscope and a 100× (1.4 NA) oil immersion objective. For excitation in the FLIM experiments, a Ti:sapphire mode-locked, pulsed infrared laser (Chameleon; Coherent) system was utilized as the multiphoton excitation source (1 W, average) tuned to 825 nm (Hoechst 33342) with pulse widths of <140 fs delivered at 90 MHz. For emission, a FLIM-specific photomultiplier tube was used and collected the spectra from 404 to 536 nm (Hoechst 33342). Fluorescence lifetime data was acquired and analyzed using previously published methods (Yaron *et al.*, 2011; Spagnol and Dahl, 2014) with a suite of software from Becker & Hickl SPC-830 for time-correlated single-photon counting with 10 ps resolution along with 220 time channels and a 10.8 ns measurement window.

The decay rate of the fluorescence lifetime can be modeled as a summation of exponential decays (Equation 1), where τ_n and a_n are the lifetime and normalized amplitude of the nth exponential decay, respectively. $I(t)$ is the number of photons detected per unit time, t, and I_0 is the offset for the background. The mean fluorescence lifetime is defined as shown in Equation 2.

$$I(t) = I_0 + \sum_n a_n e^{-t/\tau_n} \quad (1)$$

$$\tau_m = \frac{\sum_n a_n \tau_n}{\sum_n a_n} \quad (2)$$

The heat maps of the fluorescence lifetimes were created in Becker & Hickl SPCImage software along with the data analysis. For cell experiments, we segmented the nuclei in each field of view to isolate only nuclear pixel signal for data analysis using MATLAB. We analyzed the fluorescence lifetime fits using a χ^2 test, with Hoechst 33342 best modeled by a double exponential decay.

Statistical analysis

Statistical significance was measured using an unpaired, two-tailed Student's t test for data containing two groups. For data involving more than two groups, the analysis of variance (ANOVA) test was performed in order to obtain the statistical analysis for the data sets concerned. A further comparison of the groups was performed using the Tukey test to determine significant differences between groups. All statistical tests were conducted at a 5% significance level ($p < 0.05$). Prism GraphPad was used for statistical analyses. Every experiment was completed three times, and between 5 and 10 images from each group were analyzed.

Magnitudes of the mean fluorescence lifetimes were statistically compared using Student's t test. Fits of the fluorescence lifetime exponential decay were verified using a χ^2 test. For nuclear chromatin condensation state experiments using FLIM, the mean fluorescence lifetimes and associated standard deviations in the figures reflect those for segmented nuclei, with the final magnitudes resulting from pixel-to-pixel averaging within segmented nuclei across multiple nuclei per field of view and multiple fields of view per treatment condition.

ACKNOWLEDGMENTS

This work was supported by a National Science Foundation (NSF) Graduate Research Fellowship (to B.D.), National Institutes of Health Grant no. R35 GM-119617 (to D.C.), NSF CAREER award CMMI 1653299 (to D.C.), and American Heart Association Grant no. 16SDG27370007 (to D.C.).

REFERENCES

Berger L, Kolben T, Meister S, Kolben TM, Schmoeckel E, Mayr D, Mahner S, Jeschke U, Ditsch N, Beyer S (2020). Expression of H3K4me3 and H3K9ac in breast cancer. J Cancer Res Clin Oncol 146, 2017–2027.

Booth-Gauthier EA, Alcoser TA, Yang G, Dahl KN (2012). Force-induced changes in subnuclear movement and rheology. Biophys J 103, 2423–2431.

Butin-Israeli V, Adam SA, Goldman AE, Goldman RD (2012). Nuclear lamin functions and disease. Trends Genet 28, 464–471.

Chen W, Bacanamwo M, Harrison DG (2008). Activation of p300 histone acetyltransferase activity is an early endothelial response to laminar shear stress and is essential for stimulation of endothelial nitric-oxide synthase mRNA rranscription. J Biol Chem 283, 16293–16298.

Chubb JR, Boyle S, Perry P, Bickmore WA (2002). Chromatin motion is constrained by association with nuclear compartments in human cells. Curr Biol 12, 439–445.

Cunningham KS, Gotlieb AI (2005). The role of shear stress in the pathogenesis of atherosclerosis. Lab Invest 85, 9–23.

Dahl KN, Booth-Gauthier EA, Ladoux B (2010). In the middle of it all: mutual mechanical regulation between the nucleus and the cytoskeleton. J Biomech 43, 2–8.
Damodaran K, Venkatachalapathy S, Alisafaei F, Radhakrishnan AV, Jokhun DS, Shenoy VB, Shivashankar GV (2018). Compressive force induces reversible chromatin condensation and cell geometry–dependent transcriptional response. Mol Biol Cell 29, 3039–3051.
Danielsson BE, Peters HC, Bathula K, Spear LM, Noll NA, Dahl KN, Conway DE (2022). Progerin-expressing endothelial cells are unable to adapt to shear stress. Biophys J 121, 620–628.
Deguchi S, Maeda K, Ohashi T, Sato M (2005). Flow-induced hardening of endothelial nucleus as an intracellular stress-bearing organelle. J Biomech 38, 1751–1759.
Denais CM, Gilbert RM, Isermann P, McGregor AL, Te Lindert M, Weigelin B, Davidson PM, Friedl P, Wolf K, Lammerding J (2016). Nuclear envelope rupture and repair during cancer cell migration. Science 352, 353–358.
Dreger M, Madrazo E, Hurlstone A, Redondo-Muñoz J (2019). Novel contribution of epigenetic changes to nuclear dynamics. Nucleus 10, 42–47.
Dunn J, Qiu H, Kim S, Jjingo D, Hoffman R, Kim CW, Jang I, Son DJ, Kim D, Pan C, *et al*. (2014). Flow-dependent epigenetic DNA methylation regulates endothelial gene expression and atherosclerosis. J Clin Invest 124, 3187–3199.
Dunn J, Simmons R, Thabet S, Jo H (2015a). The role of epigenetics in the endothelial cell shear stress response and atherosclerosis. Int J Biochem Cell Biol 67, 167–176.
Dunn J, Thabet S, Jo H (2015b). Flow-dependent epigenetic DNA methylation in endothelial gene expression and atherosclerosis. Arterioscler Thromb Vasc Biol 35, 1562–1569.
Fedorova E, Zink D (2009). Nuclear genome organization: common themes and individual patterns. Curr Opin Genet Dev 19, 166–171.
Fejes Tóth K, Knoch TA, Wachsmuth M, Frank-Stöhr M, Stöhr M, Bacher CP, Müller G, Rippe K (2004). Trichostatin A-induced histone acetylation causes decondensation of interphase chromatin. J Cell Sci 117, 4277–4287.
Furusawa T, Rochman M, Taher L, Dimitriadis EK, Nagashima K, Anderson S, Bustin M (2015). Chromatin decompaction by the nucleosomal binding protein HMGN5 impairs nuclear sturdiness. Nat Commun 6, 6138.
Geyer PK, Vitalini MW, Wallrath LL (2011). Nuclear organization: taking a position on gene expression. Curr Opin Cell Biol 23, 354–359.
Goldberg AD, Allis CD, Bernstein E (2007). Epigenetics: a landscape takes shape. Cell 128, 635–638.
Hahn C, Schwartz MA (2009). Mechanotransduction in vascular physiology and atherogenesis. Nat Rev Mol Cell Biol 10, 53–62.
Hampoelz B, Azou-Gros Y, Fabre R, Markova O, Puech PH, Lecuit T (2011). Microtubule-induced nuclear envelope fluctuations control chromatin dynamics in *Drosophila* embryos. Development 138, 3377–3386.
Igolkina AA, Zinkevich A, Karandasheva KO, Popov AA, Selifanova MV, Nikolaeva D, Tkachev V, Penzar D, Nikitin DM, Buzdin A (2019). H3K4me3, H3K9ac, H3K27ac, H3K27me3 and H3K9me3 histone tags suggest distinct regulatory evolution of open and condensed chromatin landmarks. Cells 8, 1034.
Illi B, Nanni S, Scopece A, Farsetti A, Biglioli P, Capogrossi MC, Gaetano C (2003). Shear stress-mediated chromatin remodeling provides molecular basis for flow-dependent regulation of gene expression. Circ Res 93, 155–161.
Isermann P, Lammerding J (2013). Nuclear mechanics and mechanotransduction in health and disease. Curr Biol 23, R1113–R1121.
Iyer KV, Pulford S, Mogilner A, Shivashankar GV (2012). Mechanical activation of cells induces chromatin remodeling preceding MKL nuclear transport. Biophys J 103, 1416–1428.
Jiang Y, Ji JY (2018). Expression of nuclear lamin proteins in endothelial cells is sensitive to cell passage and fluid shear stress. Cell Mol Bioeng 11, 53–64.
Jiang YZ, Manduchi E, Jiménez JM, Davies PF (2015). Endothelial epigenetics in biomechanical stress: disturbed flow-mediated epigenomic plasticity in vivo and in vitro. Arterioscler Thromb Vasc Biol 35, 1317–1326.
Ko KA, Fujiwara K, Krishnan S, Abe JI (2017). En face preparation of mouse blood vessels. J Vis Exp 2017, e55460.
Krause M, Te Riet J, Wolf K (2013). Probing the compressibility of tumor cell nuclei by combined atomic force–confocal microscopy. Phys Biol 10, 065002.
Ku KH, Subramaniam N, Marsden PA (2019). Epigenetic determinants of flow-mediated vascular endothelial gene expression. Hypertension 74, 467–476.
Küpper K, Kölbl A, Biener D, Dittrich S, von Hase J, Thormeyer T, Fiegler H, Carter NP, Speicher MR, Cremer T, *et al*. (2007). Radial chromatin positioning is shaped by local gene density, not by gene expression. Chromosoma 116, 285–306.
Lee DY, Chiu JJ (2019). Atherosclerosis and flow: roles of epigenetic modulation in vascular endothelium. J Biomed Sci 26, 1–17.
Lee DY, Lee CI, Lin TE, Lim SH, Zhou J, Tseng YC, Chien S, Chiu JJ (2012). Role of histone deacetylases in transcription factor regulation and cell cycle modulation in endothelial cells in response to disturbed flow. Proc Natl Acad Sci USA 109, 1967–1972.
Lee DY, Lin TE, Lee CI, Zhou J, Huang YH, Lee PL, Shih YT, Chien S, Chiu JJ (2017). MicroRNA-10a is crucial for endothelial response to different flow patterns via interaction of retinoid acid receptors and histone deacetylases. Proc Natl Acad Sci USA 114, 2072–2077.
Lin K, Hsu PP, Chen BP, Yuan S, Usami S, Shyy JYJ, Li YS, Chien S (2000). Molecular mechanism of endothelial growth arrest by laminar shear stress. Proc Natl Acad Sci USA 97, 9385–9389.
Luo X, Liu Y, Kubicek S, Myllyharju J, Tumber A, Ng S, Che KH, Podoll J, Heightman TD, Oppermann U, *et al*. (2011). A selective inhibitor and probe of the cellular functions of Jumonji C domain-containing histone demethylases. J Am Chem Soc 133, 9451–9456.
Mearini G, Fackelmayer FO (2006). Local chromatin mobility is independent of transcriptional activity. Cell Cycle 5, 1989–1995.
Miroshnikova YA, Wickström SA (2022). Mechanical forces in nuclear organization. Cold Spring Harb Perspect Biol 14, a039685.
Nava MM, Miroshnikova YA, Biggs LC, Whitefield DB, Metge F, Boucas J, Vihinen H, Jokitalo E, Li X, García Arcos JM, *et al*. (2020). Heterochromatin-driven nuclear softening protects the genome against mechanical stress-induced damage. Cell 181, 800–817.e22.
Pajerowski JD, Dahl KN, Zhong FL, Sammak PJ, Discher DE (2007). Physical plasticity of the nucleus in stem cell differentiation. Proc Natl Acad Sci USA 104, 15619–15624.
Spagnol ST, Armiger TJ, Dahl KN (2016). Mechanobiology of chromatin and the nuclear interior. Cell Mol Bioeng 9, 268–276.
Spagnol ST, Dahl KN (2014). Active cytoskeletal force and chromatin condensation independently modulate intranuclear network fluctuations. Integr Biol (Camb) 6, 523–531.
Spagnol ST, Dahl KN (2016). Spatially resolved quantification of chromatin condensation through differential local rheology in cell nuclei fluorescence lifetime imaging. PLoS One 11, e0146244.
Stephens AD (2020). Chromatin rigidity provides mechanical and genome protection. Mutat Res - Fundam Mol Mech Mutagen 821, 111712.
Stephens AD, Banigan EJ, Adam SA, Goldman RD, Marko JF (2017). Chromatin and lamin A determine two different mechanical response regimes of the cell nucleus. Mol Biol Cell 28, 1984–1996.
Stephens AD, Liu PZ, Banigan EJ, Almassalha LM, Backman V, Adam SA, Goldman RD, Marko JF (2018). Chromatin histone modifications and rigidity affect nuclear morphology independent of lamins. Mol Biol Cell 29, 220–233.
Suo J, Ferrara DE, Sorescu D, Guldberg RE, Taylor WR, Giddens DP (2007). Hemodynamic shear stresses in mouse aortas: implications for atherogenesis. Arterioscler Thromb Vasc Biol 27, 346–351.
Tzima E, Irani-Tehrani M, Kiosses WB, Dejana E, Schultz DA, Engelhardt B, Cao G, DeLisser H, Schwartz MA (2005). A mechanosensory complex that mediates the endothelial cell response to fluid shear stress. Nature 437, 426–431.
van der Meer AD, Poot AA, Feijen J, Vermes I (2010). Analyzing shear stress-induced alignment of actin filaments in endothelial cells with a microfluidic assay. Biomicrofluidics 4, 011103.
Wojciak-Stothard B, Ridley AJ (2003). Shear stress–induced endothelial cell polarization is mediated by Rho and Rac but not Cdc42 or PI 3-kinases. J Cell Biol 161, 429–439.
Yaron PN, Holt BD, Short PA, Lösche M, Islam MF, Dahl KN (2011). Single wall carbon nanotubes enter cells by endocytosis and not membrane penetration. J Nanobiotechnol 9, 1–15.
Yoshida M, Kijima M, Akita M, Beppu T (1990). Potent and specific inhibition of mammalian histone deacetylase both in vivo and in vitro by trichostatin A. J Biol Chem 265, 17174–17179.
Zhou J, Li YS, Wang KC, Chien S (2014). Epigenetic mechanism in regulation of endothelial function by disturbed flow: induction of DNA hypermethylation by DNMT1. Cell Mol Bioeng 7, 218–224.
Zink D, Fischer AH, Nickerson JA (2004). Nuclear structure in cancer cells. Nat Rev Cancer 4, 677–687.